PAPER

Simulation of pre-breakdown discharges in high-pressure air: II. Effect of surface protrusions

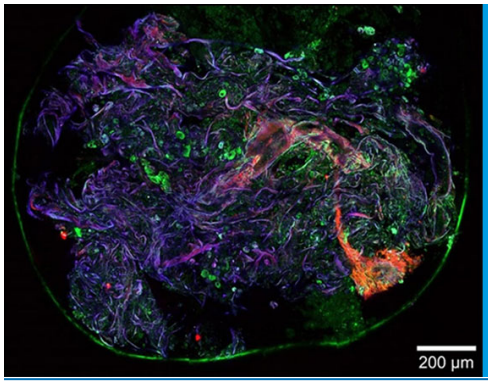

IOP Publishing Journal of Physics D: Applied Physics
J. Phys. D: Appl. Phys. **54** (2021) 255203 (10pp) https://doi.org/10.1088/1361-6463/abf372

Simulation of pre-breakdown discharges in high-pressure air: II. Effect of surface protrusions

N G C Ferreira[1,2], G V Naidis[3] and M S Benilov[1,2,*]

[1] Departamento de Física, FCEE, Universidade da Madeira, Largo do Município, 9000 Funchal, Portugal
[2] Instituto de Plasmas e Fusão Nuclear, Instituto Superior Técnico, Universidade de Lisboa, 1041 Lisboa, Portugal
[3] Joint Institute for High Temperatures, Russian Academy of Sciences, Moscow 125412, Russia

E-mail: benilov@staff.uma.pt

Received 8 February 2021, revised 13 March 2021
Accepted for publication 30 March 2021
Published 14 April 2021

Abstract

Analysis of deviations from the similarity law, observed at high and very high pressures in experiments on discharge ignition and breakdown in corona-like configurations, can serve as a useful, albeit inevitably indirect, source of information about microprotrusions on the surface of the electrodes. In this work, such analysis was performed by means of 2D numerical modelling. Conical or cylindrical protrusions on the surface of the inner electrode were studied and the kinetic scheme includes the electrons, one species of positive ions, and negative ions O_2^-, O^-, and O_3^-. It is shown that the deviations from the similarity law, observed in the experiment, may indeed be attributed to enhanced ionization of air molecules in regions of amplified electric field near the microprotrusions. A qualitative agreement with the experiment in all the cases is achieved for protrusion heights of the order of 50 μm. Such values may appear rather high, however there is no other explanation in sight at present. The enhancement of the field electron emission from the surface of the negative electrode due to the amplification of the electric field on the microprotrusion was estimated and found insignificant in the range of values of the protrusion aspect ratio where the enhanced ionization in the gas phase is already appreciable.

Keywords: gas discharge modelling, surface protrusions, breakdown of high-pressure air

(Some figures may appear in colour only in the online journal)

1. Introduction

A 'minimal' kinetic model of plasmachemical processes in low-current discharges in high-pressure air was formulated and validated in the preceding work [1]. In this work, the model is used for analysis of deviations from the similarity law, observed at high and very high pressures in experiments on discharge ignition and breakdown in corona-like configurations.

It is well known that current–voltage characteristics of field electron emission from cold cathodes in vacuum follow approximately the Fowler-Nordheim formula with the applied electric field being multiplied by the so-called field enhancement factor, which is of the order of 10^2 or higher; e.g. reviews [2–4] and references therein. Various mechanisms for the enhancement have been postulated, the most popular being amplification of the applied (average) electric field by microprotrusions present on the cathode surface. The conventional problem with this hypothesis is that in order to explain the aforementioned values of the enhancement factor, the microprotrusions are assumed to be quite slender (needle-like), and such protrusions are not normally seen on electrode surfaces; e.g. section 3.1 of [2] and [4]. Another popular mechanism is a local reduction of the work function of the cathode material, caused by, e.g. lattice defects or adsorbed atoms.

* Author to whom any correspondence should be addressed.

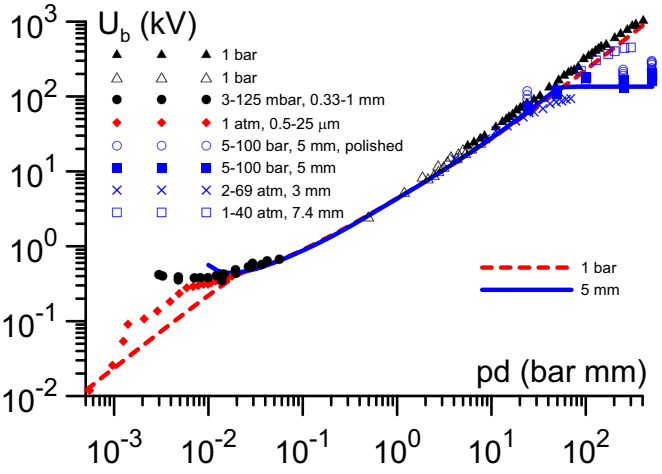

Figure 1. Breakdown voltage in uniform field in air for various air pressures p and gap widths d. Full triangles, open triangles, full circles: data from figure C1 of [7] (figure 5.23 of the book [8]). Diamonds: data from figure 6 of [9]. Open circles, full squares: data from figure 7 of [6]. Crosses: data from figure 15 of [10]. Open squares: data from figure 6 of [11]. Lines: modelling with account of enhanced field emission with $\beta = 50$. Adapted from [12].

However, this effect seems to be insufficient to explain the observed values of the field emission current; e.g. [4, 5]. Other interesting hypotheses proposed in the literature include 'non-metallic' electron emission mechanism [2] and enhancement of field emission by waves confined to the metal surface (plasmons) [4]. Thus, there is still no widely accepted understanding, in spite of several decades of active research, and this hinders the prevention of the vacuum breakdown in technical devices, e.g. in particle accelerators.

The effect of enhanced field emission from the cathode surface was considered also in gas discharge physics, in particular, in connection with deviations of measured breakdown voltage of plane-parallel gaps from Paschen's law. An example is shown in figure 1. Triangles and full circles represent measurements in medium gaps and pressures and constitute the well-known Paschen curve. Diamonds represent measurements in microgaps at atmospheric pressure; the breakdown voltage is substantially lower than the voltage determined by Paschen's law. Open circles, squares, and crosses represent measurements at very high pressures, which are substantially lower than the voltage determined by Paschen's law as well. Note that the experimental data [6] have been obtained in a concentric-cylinder geometry, rather than in the plane-parallel geometry as all the other data shown in figure 1; however, the cylinder radii (90 mm and 95 mm) were much larger than the gap width, thus the nonuniformity of the electric field was negligible.

Deviations from the Paschen law occurring at atmospheric pressure in microgaps are important for operation of micro-electromechanical and nanoelectromechanical systems and are under intensive investigation; e.g. [13–22] . Such deviations are conventionally described by introducing a field enhancement factor β into the Fowler–Nordheim field emission equation and estimating β by fitting experimental data on gas breakdown; e.g. values $\beta = 50$ and $\beta = 55$ are considered in [23] and [13, 19], respectively. As an example, results of computations [12] of the self-sustainment (breakdown) voltage with $\beta = 50$ are shown by the dashed line in figure 1 for $p = 1$ bar over a wide range of gap widths d. (Note that the computations [12] have been performed by means of a model of low-current discharges in air, similar to the 'minimal' model [1] and described in the next section. However, the computations [12] refer to the parallel-plate geometry and therefore were one-dimensional. The electron emission current was set equal to sum of the field emission current, evaluated with the electric field at the cathode surface enhanced by a factor of β and the work function of 4.5 eV, and the secondary electron emission with the effective coefficient of 10^{-4}. The voltage corresponding to the initiation of a self-sustaining discharge was computed, which for the parallel-plate geometry is usually assumed to coincide with the breakdown voltage). As expected, the computed breakdown voltage follows Paschen's law for $d \gtrsim 20$ μm and is below the Paschen values for smaller gap widths, in qualitative agreement with the experimental data.

Note that the field enhancement factor used in such-type macroscopic modelling is not the same as the one determined by fitting field electron emission currents from cold cathodes in vacuum by Fowler-Nordheim plots, which refers not to the entire cathode surface but rather to an 'emission area', extracted from the Fowler–Nordheim plot (e.g. [24]). On the other hand, the field enhancement factor determined by fitting field electron emission currents by the Fowler-Nordheim plots is usually much higher than the above-mentioned value of around 50, which should to a certain extent compensate the difference between the areas.

Deviations from the Paschen law occurring at very high pressures, seen in Figure 1 in the range pd $\gtrsim 50$ bar mm, have been known for several decades [10, 23, 25]: as the air pressure p in high-voltage air insulation systems increases, the breakdown voltage first increases proportionally to p, then the increase slows down and starting from pressures of the order of 10 atm becomes very slow. Recent surge of interest in this topic [6, 26] is motivated by the possibility to use high-pressure air as a replacement for SF_6 for high-voltage insulation, due to removal of SF_6 from industrial applications for environmental reasons.

The early authors [10, 23, 25] hypothesized that the reason of these deviations is the field emission from the negative electrode enhanced by microno nuniformities. Assuming this hypothesis, one can try to describe this effect in the same way as indicated above for the case of microgaps, i.e. by introducing a field enhancement factor β into the electron emission equation. As an example, the solid line in figure 1 depicts the breakdown voltage computed with $\beta = 50$ for $d = 5$ mm over a wide range of pressures. As expected, the breakdown voltage follows Paschen's law for $p \lesssim 10$ bar and saturates for higher pressures, in qualitative agreement with the experimental data. It should be stressed that the value $\beta = 50$, used in these computations, is the same as the value of β that gave the qualitative agreement with the experiment for microgaps (the dashed line). We note for completeness that in the range pd $\lesssim 10^{-2}$ bar mm the breakdown voltage computed for

$d = 5$ mm (the solid line) is higher than values given by the experimental Paschen's law (full circles). This can be attributed to the local electric field approximation, used in the modelling for evaluation of the transport and kinetic coefficients of electrons, loosing its validity: d is no longer large compared with the electron energy relaxation length and the electron distribution function has to be described by a non-local model [27–30].

The saturation of the breakdown voltage for pressures $p \gtrsim 10$ bar may be understood as follows in the framework of this hypothesis. Field emission comes into play for cathodes with a work function of 3–4 eV at a local field strength at the cathode surface exceeding 10^9 V m^{-1}. For $\beta = 50$, this corresponds to an average field of the order of 2×10^7 V m^{-1} and to a breakdown voltage of the order of 200 (d/ cm) kV. For $d = 5$ mm, this gives the breakdown voltage of the order of 100 kV, comparable with the value of 130 kV at which the solid line in figure 1 reaches saturation. It is interesting to note that modelling for the gap $d = 0.5$ mm gave the saturation voltage of 13 kV, which, on the one hand, agrees in order of magnitude with the above simple estimate, and on the other hand means that the computed breakdown voltage starts deviating from the Paschen law at lower pd values than the data for the 5 mm gap shown by the solid line. Similarly, modelling for $p = 10$ bar gave a line which is shifted by an order of magnitude in the direction of higher pd with respect to the dotted line, computed for 1 bar, and approaches the Paschen curve at a larger pd, significantly to the right of the minimum. Thus, both a decrease in the gap length d and an increase in pressure p narrow the range of applicability of the Paschen law.

Another early author [11] made strong arguments explaining the saturation of the breakdown voltage at high pressures not by field emission (or at least not only by field emission), but rather by the enhanced ionization of neutral gas molecules in regions of increased electric field near the protrusions on the surface of the positive or negative electrodes. Recent workers [6, 26] supported this hypothesis by evaluation of the ionization integral.

Thus, the deviations of measured breakdown voltage of plane-parallel gaps from Paschen's law, observed in microgaps and at very high pressures, may be described in the same way as deviations of field electron emission from cold cathodes in vacuum from the Fowler-Nordheim formula, i.e. in terms of enhancement of electron emission that may occur due a variety of reasons, such as amplification of the applied electric field by microprotrusions present on the cathode surface, local reduction of the work function of the cathode material, 'nonmetallic' electron emission mechanism, plasmons. There is an alternative explanation for deviations from Paschen's law at very high pressures, and this explanation is specifically related to the supposed existence of microprotrusions on the electrode surfaces: enhanced ionization of neutral gas in regions near protrusions.

The situation may be clarified by considering deviations from the similarity law observed at very high pressures in corona inception and breakdown voltages for discharges on positive cylindrical electrodes of small radii [11, 31]: cathodic phenomena are irrelevant and enhanced ionization of neutral gas in regions near protrusions on the anode surface appears to be the only possible explanation. In this work, the measurements [11, 31] are analyzed from this point of view by means of numerical modelling. It is shown that the deviations from the similarity law, observed in the experiment, may indeed be attributed to enhanced ionization of air molecules in regions of enhanced electric field near microprotrusions on the anode surface. Given the absence of any other plausible explanation, this conclusion may be considered as an indirect evidence of the existence of microprotrusions on the electrode surface. Moreover, analysis of the experimental data allows estimating dimensions of the microprotrusions in conditions of these experiments.

The outline of the paper is the following. Section 2 contains an overview of the model of low-current discharges in high-pressure air and the kinetic scheme used. Results of computation of the ignition voltage (voltage corresponding to the initiation of a self-sustaining discharge) in high-pressure air under conditions simulating the measurements [11, 31] are reported and discussed in section 3. Conclusions are summarized in section 4.

2. The model

The model and the kinetic scheme of low-current discharges in air at pressures of the order of atmospheric and higher, used in this work, is similar to the 'minimal' model [1], with the changes introduced in [32]. In brief, the model includes equations of conservation and transport of charged species, written in the drift-diffusion approximation, and the Poisson equation. The kinetic scheme includes the following charged species: the electrons, one effective species of positive ions, and the negative ions O_2^-, O^- and O_3^-. The ions produced in air by the electron impact ionization are N_2^+ and O_2^+. Ions O_2^+ are generated also by the photoionization, which is produced by UV radiation emitted by N_2 molecules excited by electron impact. The N_2^+ ions in air at pressures about 1 atm and higher are rapidly converted into O_2^+. One channel of such conversion is the fast charge transfer reaction $N_2^+ + O_2 \rightarrow O_2^+ + N_2$. Another channel comprises a three-body conversion process of N_2^+ and N_2 molecules into the N_4^+ ions, followed by the charge transfer from N_4^+ to O_2. Therefore, the positive ions in the ionization (active) zone are represented mostly by O_2^+.

The plasmachemical processes include electron impact ionization, photoionization, two-body (dissociative) attachment, three-body attachment, photoionization, collisional detachment from O_2^-, associative detachment from O^-, charge transfer from O^- to O_2^-, conversion of O^- to O_3^-, and ion-ion and electron-ion recombination. The photoionization was evaluated by means of the three-exponential Helmholtz model [33]. The possible formation in the drift zone of the complex ions O_4^+, O_4^- and, in the case of humid air, cluster ions (comprising one or several H_2O molecules) [34, 35] was taken into account in the choice of the mobility of the effective positive ion species and the ions O_2^- as discussed in [32]. The diffusion coefficient of each ion species is related to its mobility through Einstein's relation with the corresponding ion temperature, which

was evaluated by means of the Wannier equation. Since the modelling of this work is aimed at computing the discharge ignition voltage and the neutral gas is still cold at the discharge ignition, the neutral gas temperature is set equal to 300 K. The boundary conditions are conventional and the same as in [1] with exception of the boundary condition for electrons at the cathode, where, in addition to the secondary electron emission, also taken into account are electron losses to the cathode due to the chaotic motion.

Note that the 'minimal' model was validated in [1] by a comparison of the computed inception voltage of corona discharges with several sets of experimental data on positive and negative glow coronas between concentric cylinders, over a wide range of pressures and diameters of the cylinders, and on positive coronas in the rod-to-plane configuration. The changes introduced to the model in [32] did not affect the inception voltage, the parameter computed in [1], and the updated model was validated by a comparison of the computed steady-state corona parameters with time-averaged measurements data in DC corona discharges in point-plane gaps in ambient air over a wide range of currents of both voltage polarities and various gap lengths.

The model was implemented on the computational platform COMSOL Multiphysics® and solved with the use of stationary solvers. The following interfaces were used: electrostatics (the Poisson equation), transport of diluted species (the equations of conservation and transport of charged species), with the default consistent stabilization (streamline and crosswind diffusion) activated, and coefficient form (the Helmholtz equations). While in the preceding work [1] the logarithmic formulation of the species conservation equations was used, which is a frequent choice in the modelling of cold gas discharges, the original formulation, where the dependent variables are the species number densities, was used in this work. The reason for this is that the original formulation has been found to be much more efficient for the steady-state modelling required for the computation of the discharge ignition voltage, reported in this work, similarly to what was found in the corona simulations reported in [32].

The aim of the modelling was to compute the voltage corresponding to the initiation of a self-sustaining discharge (the ignition voltage) for each discharge geometry over a wide range of gas pressures. The initial step for each geometry was to find the ignition voltage for one pressure value using the eigenvalue approach developed in [36]. After that, the control parameter was switched from the discharge voltage to the discharge current and the gas pressure was gradually varied until the whole range of pressure values of interest has been covered. The solution computed for each value of gas pressure was used as an initial approximation for the computation with the next value. The discharge current was kept fixed at this stage and it was ensured that the current is sufficiently low not to affect the computed voltage.

3. Results and discussion

The aim of modelling of this work is to study qualitatively the effect of microprotrusions, present on the surface of the inner electrode, over the discharge ignition voltage under conditions of experiments with concentric cylinder electrodes in high to very high pressure air, reported in [11, 31].

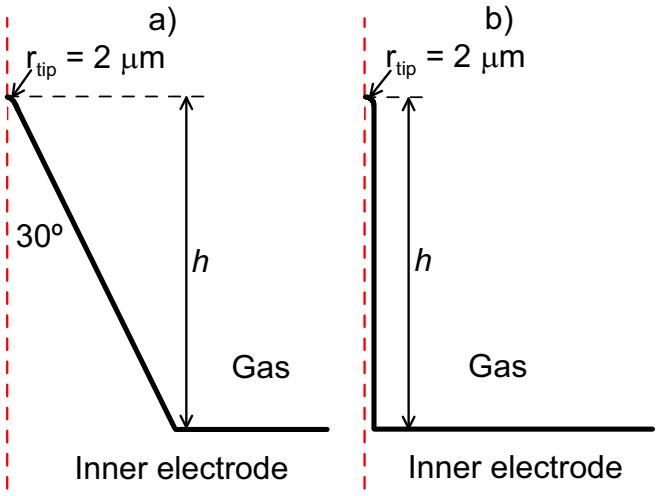

Figure 2. Schematic representation of the conical (a) and cylindrical (b) protrusions.

If the electrodes were smooth, the concentric cylinder geometry could be simulated using a one-dimensional (1D) model. 3D models are, strictly speaking, required in order to study the effect of protrusions on the surface of the inner cylinder, except for a special case of protrusions having the shape of long ridges parallel to the cylinder axis, where a 2D model is sufficient. However, multidimensional modelling in the general case requires resolving a thin ionization zone along the entire surface of the inner electrode, and this makes 3D models heavy computationally, so their use for a qualitative investigation is unwarranted.

In this work, concentric sphere electrodes are considered with a single cylindrical or conical protrusion on the surface of the inner electrode. Due to the axial symmetry, the modeling is 2D and therefore not too heavy. Since different protrusions come into play under different conditions, the presence of several microprotrusions acting in close proximity is unlikely. (This may be untrue for arrays of identical protrusions; see the beginning of section 4 below.) On the other hand, microprotrusions that are not located close to each other do not interact. Since the electric field distributions in the vicinity of small protrusions of the same geometry on cylindrical and spherical electrodes are close to each other, the assumed computational geometry should allow studying the influence of protrusions at least qualitatively.

Results reported in this work refer to conical protrusions with a 60° full aperture angle and a spherical tip with a radius of 2 μm and cylindrical protrusions of a radius of 2 μm and a (half-)spherical tip of the same radius, both of which are schematically shown in figure 2. The protrusion height is several tens of micrometers in both cases. It should be stressed that while the cylindrical protrusion is slender and in line with protrusions usually considered in the modelling of vacuum breakdown (e.g. [37]), the conical protrusion, proposed in [38], is not slender and the electric field amplification is due to high

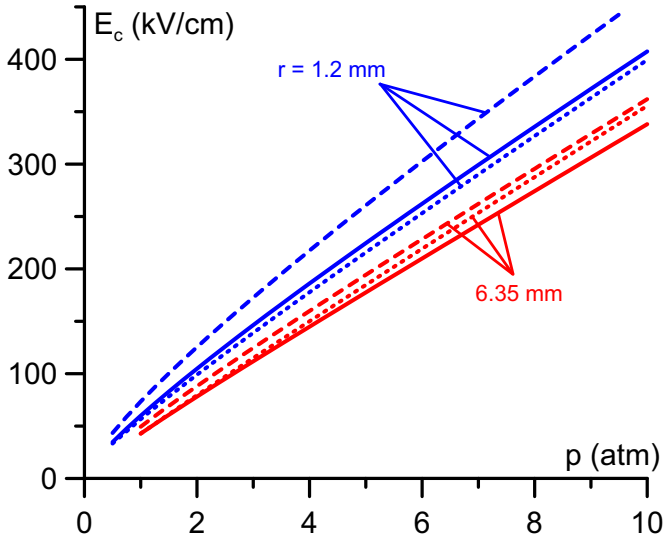

Figure 3. Ignition field on a positive electrode without protrusions for two values of the electrode radius r. Solid: modelling, concentric cylinder electrodes. Dotted: empirical Peek's formula for the ignition field of a positive corona discharge between concentric cylinder electrodes. Dashed: modelling, concentric sphere electrodes.

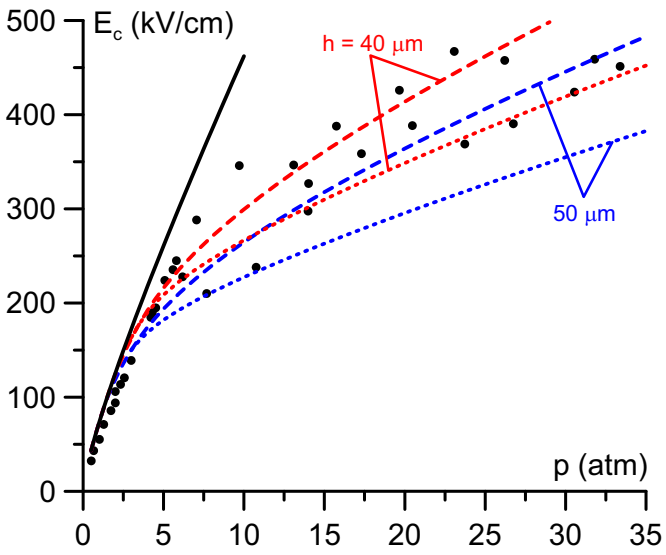

Figure 4. Ignition field on a positive electrode, $r = 1.2$ mm. Lines: modelling without account of protrusions (solid) and with account of a conical (dashed) or cylindrical (dotted) protrusion of height h. Points: experiment [31].

values of the ratio of the height of the protrusion to the tip radius.

Let us designate by r and R the radii of the inner and outer electrodes, respectively. The results reported in this work simulate experiments with the following values of these parameters: $r = 1.2$ mm, $R = 48.75$ mm and $r = 3.18$ mm, $R = 48.75$ mm, which are geometries studied experimentally in [31], and $r = 6.35$ mm, $R = 13.5$ mm, which is a geometry studied experimentally in [11]. In the modelling, the radius of the inner sphere was chosen equal to the radius of the inner cylinder in the experiment being simulated. The radius of the outer sphere was chosen equal to the radius of the outer cylinder in the modelling of the experiment [11]. In the modelling of the experiment [31], the radius of the outer sphere was chosen such that the discharge gap be equal to 10 mm, instead of about 46–48 mm as in the experiment. This reduction of the computation domain allowed reducing the number of elements of the numerical mesh. On the other hand, this reduction did not introduce a significant error, since the effect of the radius of the outer electrode on the ignition field is weak, which is well known (e.g. R does not appear in Peek's formula for the ignition field of a positive corona discharge between concentric cylinder electrodes) and was verified in the modelling of this work.

The comparison parameter is E_c the macroscopic ignition electric field at the inner electrode, defined as $E_c = U_c/[r\ln(R/r)]$ for concentric cylinders and $E_c = U_c/[r(1-r/R)]$ for concentric spheres, where U_c is the ignition voltage.

Let us start with verifications for the case without protrusions. The solid lines in figure 3 represent the ignition field on a positive electrode for concentric cylinder electrodes, computed by means of the model used in this work without account of protrusions, for two of the above-mentioned geometries: $r = 1.2$ mm, $R = 48.75$ mm and $r = 6.35$ mm, $R = 13.5$ mm. The dotted lines depict the corona ignition field at the surface of a positive inner cylinder (wire) given by equation (1) of [31], which is one of variants of empirical Peek's formula. The solid and dotted lines are very close to each other for both geometries; an additional validation of the model.

The dashed lines in figure 3 represent the ignition field calculated for concentric sphere electrodes with $r = 1.2$ mm, $R = 11.2$ mm and $r = 6.35$ mm, $R = 13.5$ mm. The difference between the ignition fields computed for the concentric sphere and cylinder electrodes is relatively small. As expected, the difference is smaller for the wider electrode, $r = 6.35$ mm; cf e.g. figure 4 of [39].

The effect of protrusions is illustrated by figures 4–7. The lines in these figures were computed for concentric sphere electrodes without account of protrusions (solid) or with account of a conical or cylindrical protrusion of a height h on the inner electrode (dashed and dotted, respectively). The points in figures 4 and 5 represent the discharge ignition field estimated from the experimental corona-starting voltage reported in [31], in the pressure range $p \lesssim 5$ atm, where a preceding corona discharge was observed prior to sparkover, and from the sparkover voltage [31] for higher pressures, where a preceding corona discharge was not observed. The points in figures 6 and 7 represent the discharge ignition field estimated from the experimental breakdown voltage [11].

Figures 4–6 refer to the ignition field on positive electrodes of different radii. In all the cases, the computed ignition field is close to the experimental values in the pressure range of 0.5–3 atm, where the effect of protrusions is negligible and the similarity law and Peek's formula hold. As expected, the presence of a protrusion results in a reduction of the macroscopic ignition field due a higher local electric field and, consequently,

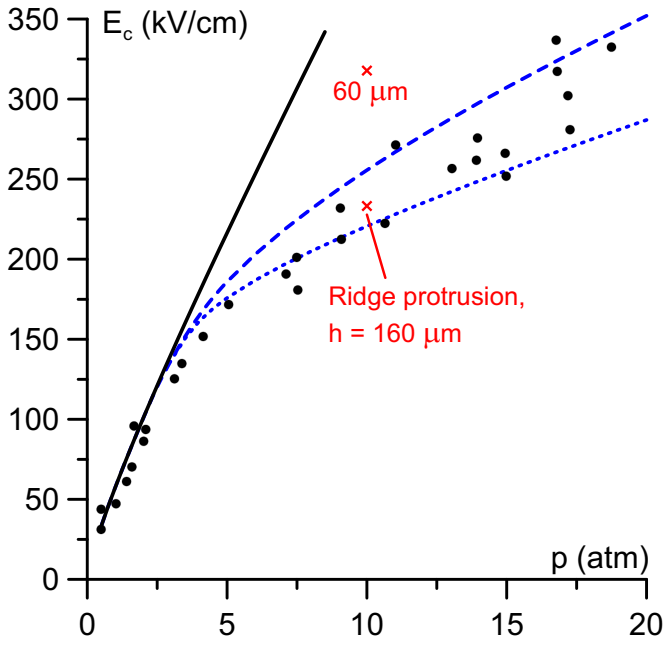

Figure 5. Ignition field on a positive electrode, $r = 3.18$ mm. Lines: modelling without account of protrusions (solid) and with account of a conical (dashed) or cylindrical (dotted) protrusion of a height of 50 μm. Crosses: modelling, concentric cylinder electrodes with a ridge protrusion of height h. Points: experiment [31].

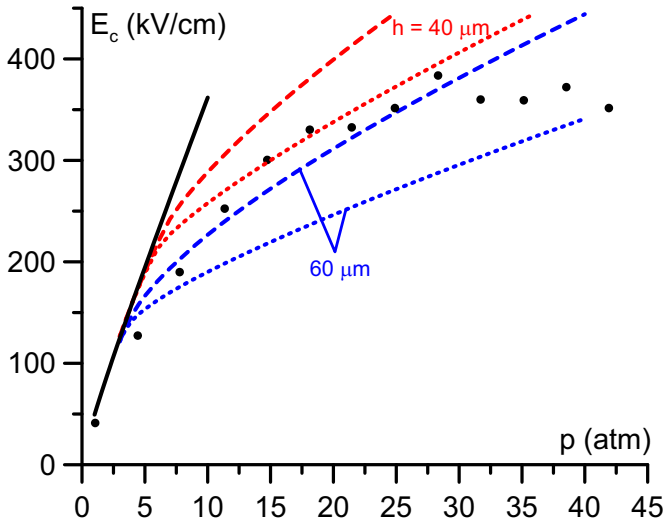

Figure 6. Ignition field on a positive electrode, $r = 6.35$ mm. Lines: modelling without account of protrusions (solid) and with account of a conical (dashed) or cylindrical (dotted) protrusion of height h. Points: experiment [11].

substantially increased ionization in the vicinity of the protrusion. The effect comes into play at pressures of the order of 5 atm. As expected, the larger the assumed protrusion height h, the lower the computed ignition field is. A cylindrical protrusion produces a stronger effect than a conical protrusion of the same height, although the difference is not very substantial. A qualitative agreement with the experiment in all the cases is achieved for protrusion heights of the order of 50 μm. Such

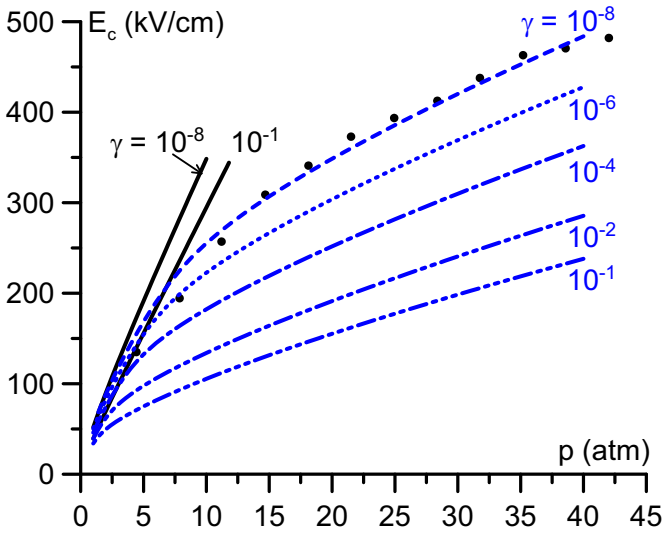

Figure 7. Ignition field on a negative electrode, $r = 6.35$ mm. Lines: modelling without account of protrusions (solid) and with account of a conical protrusion of a height of 60 μm (dashed, dotted, and dash-dotted lines), for various values of the secondary electron emission coefficient γ. Points: experiment [11].

values seem rather high, however there is no other explanation in sight at present.

For comparison purposes, also shown in figure 5 are results of simulations for concentric cylinder electrodes with a long ridge at the surface of the inner cylinder, parallel to the cylinder axis. These simulations were 2D as well, but performed in the Cartesian coordinates (x, y), rather than in the cylindrical coordinates (r, z) as the simulations for concentric sphere electrodes with a conical or cylindrical protrusion. The ridge had a 60° full aperture angle and a cylindrical rounding of a radius of 2 μm at the tip, i.e. the transversal (perpendicular to the cylinder axis) cross section of the ridge was the same as the axial cross section of the conical protrusion. The crosses in figure 5 refer to two values of the ridge height, 60 μm and 160 μm. One can see that ridge protrusions must have a bigger height than conical ones for a comparable effect.

The experimental data [11] shown in figure 6 manifest saturation of the breakdown field in the range $p \gtrsim 30$ atm, whereas the modelling does not. However, one should note that the author [11] mentioned that the measurements were uncertain at higher pressures and a reproducible breakdown voltage measurement was hard to perform.

For completeness, let us consider the effect of protrusions in the case of negative polarity (the inner cylinder being the cathode). The experimental data from [11] for the negative polarity under conditions comparable to those of figure 6 are shown in figure 7. One can see that the deviations from the similarity law for the negative polarity are qualitatively similar to those for the positive polarity, however at high pressures the breakdown voltage for the negative polarity is, somewhat surprisingly, higher than for the positive polarity. Note that a similar effect has been observed in conditioning experiments described in [40]: at application of DC high voltage to a plane-plane gap with a 4 mm diameter sphere at one of the electrodes

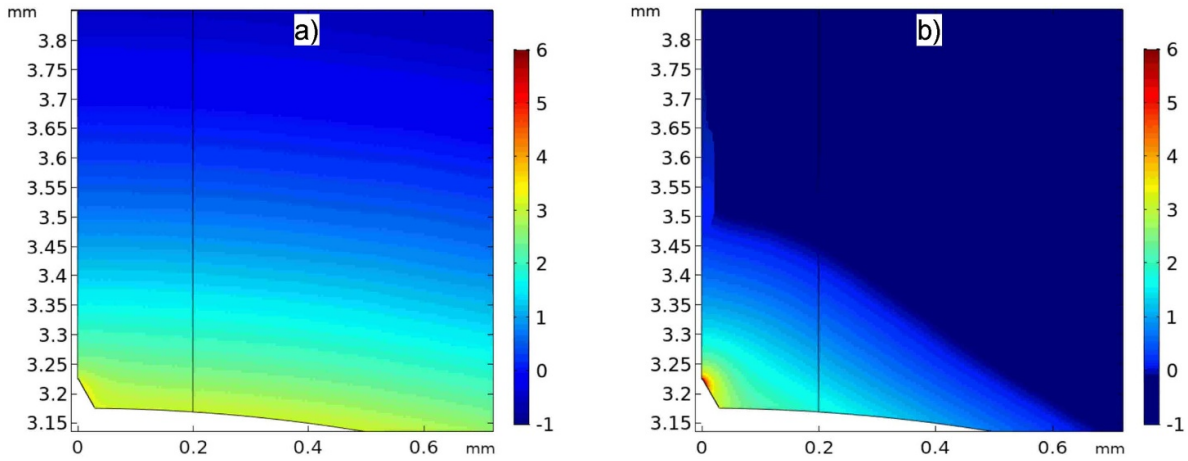

Figure 8. Bidimensional distribution of the logarithmic density of the negative ions O_2^- in the vicinity of a conical protrusion of a height of 50 μm at the surface of a positive electrode. Density in m^{-3}. Discharge current 10^{-14} A, $r = 3.18$ mm. (a): $p = 1$ atm. (b): $p = 5$ atm.

in air at pressure of 30 bar, the first breakdown voltages for a positive potential at the sphere were considerably lower than the corresponding values for the negative polarity.

In the case of negative polarity, primary electrons are supplied to the ionization zone at the inner electrode by the electron emission from the electrode surface, rather than by photoionization as in the case of positive polarity. Two electron emission mechanisms need to be considered: secondary electron emission and field emission. The modelling shown in figure 7 was performed for various values of γ the effective coefficient of secondary electron emission without account of the field emission. The ignition field on the negative electrode varies with γ as one could expect, and the presence of the protrusion significantly enhances this variation. The latter can be understood as follows. In the case without protrusions, the electric field at the cathode surface is close to the critical field, i.e. the field value at which the electron impact ionization is just sufficient to balance the electron attachment. The electron impact ionization rate coefficient grows very rapidly with the increasing electric field in this field range, and minor discharge voltage variations are sufficient to compensate significant variations in the number of primary electrons, caused by variations in γ. In the case with the protrusion, the electric field at the protrusion is appreciably higher than the critical field; the field dependence of the electron impact ionization rate coefficient in this field range is less strong, hence variations in the discharge voltage, caused by variations in γ, are more significant.

The maximum average electric field at the surface of the negative electrode under conditions of the experiment [11] is 5×10^7 V m^{-1}; cf figure 7. The electric field at the tip of a protrusion of a height of 50 μm, given by the axially symmetric electrostatic simulations, is higher by the factor of approximately 20 or 27 for the conical or cylindrical protrusions, respectively, and thus is close to 10^9 V m^{-1}. The latter value is too low for the field emission to be appreciable. Indeed, the field emission current evaluated from the axially symmetric numerical modelling for conditions of figure 7 for $p = 40$ atm is by six orders of magnitude lower than the secondary electron emission current even for the lowest γ value considered $\gamma = 10^{-8}$. Thus, the enhancement factor is not high enough or, equivalently, the aspect ratio is not sufficient for appreciable field emission. One can conclude that in these conditions the effect of the enhanced ionization of air molecules in regions of amplified electric field near microprotrusions at the cathode surface comes into play for lower values of the aspect ratio than the field emission.

As mentioned above, deviations from the similarity law for the negative and positive polarities, observed in the experiment [11], are qualitatively similar. Comparing computation results shown in figures 7 and 6, one can conclude that the effect produced by the account of the microprotrusion in the modelling for the cases of negative and positive polarities is qualitatively similar as well, in agreement with the experimental data. The fact that the experimental breakdown voltage for the negative polarity at high pressures is higher than for the positive polarity, means in terms of the modelling that the effective secondary electron emission coefficient at the surface of the negative electrode is smaller than 10^{-6}, which is a typical value characterizing photoionization in this pressure range. Indeed, the value of γ, which ensures the best agreement with the experiment in figure 7, is $\gamma = 10^{-8}$. On the other hand, this value is unusually low. This point clearly requires further experimental investigation. One could imagine, as a possible reason, a decrease of γ with increasing pressure, for example, due to the deposition of neutral gas molecules on the metal surface, or since cluster ions with a large number of water molecules, formed at high pressures, do not produce secondary electrons as efficiently as light ions.

The effect of protrusions over the computed distribution of discharge parameters along the electrode surface is illustrated by figure 8. The simulation conditions are the same as those of figure 5 with a conical protrusion of a height of 50 μm. For the atmospheric pressure (figure 8(a)), the discharge is distributed along the electrode surface in a more or less uniform way; in other words, the effect of the protrusion is minor. The

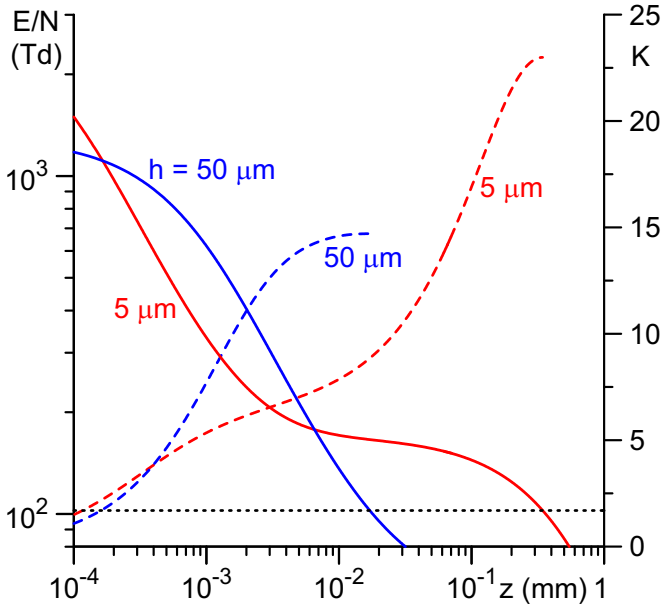

Figure 9. Distributions of the reduced electric field (solid) and the ionization integral (dashed) along the discharge axis. Dotted: critical field. Positive inner electrode, $r = 1.2$ mm, $p = 20$ atm, conical protrusions with $h = 50$ μm, $r_{\text{tip}} = 2$ μm and $h = 5$ μm, $r_{\text{tip}} = 0.2$ μm.

discharge ignition field is adequately described by Peek's formula. As pressure increases, the discharge starts concentrating in the vicinity of the protrusion (figure 8(b)) and the ignition field is lower than the value given by Peek's formula.

Although high values of the ratio of the protrusion height to the tip radius are required for electric field amplification and hence represent a necessary condition for the deviations from the similarity law at high pressures observed in [11, 31], this condition alone is not sufficient: the protrusion height must be not too small, otherwise the electric field decays at very small distances from the protrusion tip and sufficient ionization is not produced. An example is shown in figure 9. Here z is the distance measured along the discharge axis from the protrusion tip, E/N is the reduced electric field, and $K = \int_0^z \alpha_{\text{eff}}\, dz$ is the ionization integral (α_{eff} is the effective ionization coefficient evaluated using the data [1]). Data for two conical protrusions of different heights h with the same aspect ratio h/r_{tip} are shown. For the protrusion with $h = 50$ μm, the computed ignition field, $E_c \approx 364$ kV cm^{-1}, is shown in figure 4 and agrees with the experiment as seen in the latter figure. The total (evaluated along the ionization zone) ionization integral is contributed by the region of z of the order of r_{tip} ($= 2$ μm). For the protrusion with $h = 5$ μm, the electric field is higher at the protrusion tip but decays in space faster, therefore the contribution of the region of z of the order of r_{tip} ($= 0.2$ μm) to the total ionization integral is no longer dominating. Unsurprisingly, the computed ignition field, $E_c \approx 836$ kV cm^{-1}, is much higher than the experimental value shown in figure 4.

It is seen from figure 9 that the total ionization integral characterizing the ignition of corona-like discharges strongly depends on the geometry. This is an interesting illustration of the limitation of the method for evaluation of ignition potential by assuming a prescribed value for the ionization integral, which is routinely used as a substitute for numerical modelling similar to the one used in this work.

4. Summary and concluding remarks

The voltage corresponding to the initiation of a self-sustaining discharge is computed in corona-like discharge configurations with microprotrusions on the surface of the inner electrode over a wide range of pressures by means of 2D numerical modelling. The kinetic scheme includes electrons, one species of positive ions, and negative ions O_2^-, O^-, and O_3^-. In particular, the model describes, in a natural way, the enhanced ionization of air molecules in regions of amplified electric field near the microprotrusion. The aim of the modelling is to find out if the latter mechanism may be responsible for the deviations from the similarity law at high pressures, observed in the experiment.

The model was applied to conditions of corona inception and breakdown experiments on concentric cylinders over a wide pressure range described in [11, 31]. An axially symmetric geometry consisting of concentric sphere electrodes with a single cylindrical or conical microprotrusion on the surface of the inner electrode was considered. Since different protrusions come into play under different conditions, the presence of several microprotrusions acting in close proximity is unlikely. (Note that this reasoning does not apply to arrays of identical protrusions, nevertheless it is interesting to mention in this connection the recent experiments [41], which showed little effect of the number of protrusions in the array for the case of SF_6 but a more appreciable effect for the case CO_2; figures 7, 8 and 12, 13 of [41], respectively. This is an interesting point that may need to be revisited in the future.) On the other hand, microprotrusions that are not located close to each other do not interact. Therefore, the assumed computational geometry with a single protrusion should be sufficient for a qualitative study while avoiding 3D modeling, which is demanding and unwarranted at this stage. The reported results refer to conical protrusions with a 60° full aperture angle and a spherical tip with a radius of 2 μm and cylindrical protrusions of a radius of 2 μm with a half-spherical tip, the protrusion heights being of several tens of micrometers in both cases. While the cylindrical protrusion is slender, the conical protrusion is not and the electric field amplification is due to high values of the ratio of the height of the protrusion to the tip radius.

For lower pressures, in the range of 0.5–3 atm, the discharge is not appreciably affected by the presence of the protrusion and is distributed along the surface of the inner electrode in a more or less uniform way. The computed ignition field is close to the experiment and to values given by empirical Peek's formula and increases with p approximately proportionally, in agreement with the similarity law. For higher pressures, the discharge concentrates in the vicinity of the protrusion and the increase of the computed ignition field with pressure slows down, in agreement with the experimental data. The protrusion

heights necessary to achieve a qualitative agreement with the experiment are of the order of 50 μm in all the cases.

In the case where the inner electrode is positive, the enhanced ionization of air molecules in regions near microprotrusions on the electrode surface appears to be the only possible explanation for the deviations from the similarity law at high pressures, observed in the experiments [11, 31]. The qualitative agreement of the simulation results with the experiment can be considered as indirect evidence of the existence of microprotrusions and indicates what height of microprotrusion is necessary to produce the effect: on the order of tens of micrometers. The protrusions need not necessarily be slender; e.g. conical protrusions with a large (60°) aperture angle and a small tip curvature radius produce a similar effect. Ridge protrusions produce a similar effect as well, however a bigger height or a smaller tip curvature radius is required. This aspect is important since protrusions that are not slender appear to be more realistic than needle-like ones.

It should be stressed that, although high values of the ratio of the protrusion height to the tip radius are required for electric field amplification and hence represent a necessary condition for the deviations from the similarity law at high pressures observed in [11, 31], this condition alone is not sufficient: the protrusion height must be not too small, otherwise the electric field decays at very small distances from the protrusion tip and sufficient ionization is not produced. Thus, while the above-mentioned values of microprotrusion height of several tens of micrometers may appear rather high, there seems to be no other explanation at present.

The enhanced ionization of air molecules in regions near protrusions on the electrode surface explains also the deviations from the similarity law at high pressures observed in the experiments [11] in the case where the inner electrode is negative. Another mechanism that may play a role in this case is the enhanced electron emission from the cathode surface; the same mechanism which causes deviations from the Fowler-Nordheim formula in experiments on field electron emission from cold cathodes in vacuum and which may occur due a variety of reasons, such as amplification of the applied electric field by microprotrusions on the cathode surface, local reduction of the work function of the cathode material, 'nonmetallic' electron emission mechanism, plasmons. In this work, the enhancement of the field emission due to the amplification of the electric field was estimated and it was found that in the range of values of the protrusion aspect ratio where the enhanced ionization of air molecules in the gas phase comes into play the field emission is still insignificant.

Modelling of this work shows that the experiments on positive corona discharge ignition and breakdown at high and very high pressures can serve as a useful, albeit inevitably indirect, source of information about microprotrusions on the surface of electrodes. Unfortunately, the experimental information available is clearly insufficient. One of important questions to be answered is the relation between the deviations from the similarity law and the degree of polishing of the inner electrode. Note that experimental results reported in [31] refer to four values of the inner cylinder radius: 0.089 mm, 0.216 mm, 1.20 mm, and 3.18 mm. Deviations from the similarity law, found in the modelling with the same protrusion height of 50 μm, were comparable for all the four values. The deviations found in the experiment [31] were comparable for the radii of 1.20 mm and 3.18 mm (cf figures 4 and 5 above), were significantly smaller for 0.216 mm, and still smaller for 0.089 mm. Of course, microprotrusions on different cylinders need not be the same; in particular, it is unclear if 50 μm protrusions are likely to occur on a wire of a radius of 89 μm. Hopefully, the relation between the deviations from the similarity law and the degree of polishing of the inner electrode will be addressed in future experiments.

Data availability statement

All data that support the findings of this study are included within the article (and any supplementary files).

Acknowledgments

This work was supported by FCT of Portugal under project UIDP/50010/2020 and by European Regional Development Fund through the program Madeira 2014-2020 under project PlasMa-M1420-01-0145-FEDER-000016 (UMa), and by the RFBR Grant No. 20-02-00320 (JIHT). The authors are grateful to Thomas Hammer and Svetlana Gossmann of Siemens Erlangen for stimulating discussions that initiated this work, Martin Seeger of ABB Switzerland for additional information on the experiment [6], and Walter Wuensch of CERN for stimulating discussions.

ORCID iDs

N G C Ferreira https://orcid.org/0000-0001-5938-4182
G V Naidis https://orcid.org/0000-0003-2184-802X
M S Benilov https://orcid.org/0000-0001-9059-1948

References

[1] Ferreira N G C, Santos D F N, Almeida P G C, Naidis G V and Benilov M S 2019 *J. Phys. D: Appl. Phys.* **52** 355206
[2] Latham R V and Xu N S 1991 *Vacuum* **42** 1173
[3] R V Latham (ed) 1995 *High Voltage Vacuum Insulation. Basic Concepts and Technological Practice* (New York: Academic)
[4] Wuensch W 2019 *8th Int. Workshop on Mechanisms of Vacuum Arcs (Padova, Italy, 15–19 September, 2019)* p 11
[5] Sinelnikov D N 2014 PhD Thesis National Research Nuclear University 'MEPhI' (in Russian)
[6] Seeger M, Stoller P and Garyfallos A 2017 *IEEE Trans. Dielectr. Electr. Insul.* **24** 1582
[7] Dakin T W, Luxa G, Oppermann G, Vigreux J, Wind G and Winkelnkemper H 1974 *Electra* **32** 61
[8] Kuffel E, Zaengl W S and Kuffel J 2000 *High Voltage Engineering* 2nd edn (Oxford: Newnes)
[9] Dhariwal R S, Ahmad M F and Desmulliez M P Y 2001 *Proc SPIE* **4407** 172–9
[10] Cohen E H 1956 *Proc. IEEE* A **103** 57
[11] Howell A H 1939 *Electr. Eng.* **58** 193

[12] Ferreira N G C, Naidis G V and Benilov M S 2019 *8th Int. Workshop on Mechanisms of Vacuum Arcs (Padova, Italy, 15–19 September 2019)* p 18
[13] Zhang W, Fisher T S and Garimella S V 2004 *J. Appl. Phys.* **96** 6066
[14] Hourdakis E, Bryant G W and Zimmerman N M 2006 *J. Appl. Phys.* **100** 123306
[15] Go D B and Pohlman D A 2010 *J. Appl. Phys.* **107** 103303
[16] Go D B and Venkattraman A 2014 *J. Phys. D: Appl. Phys.* **47** 503001
[17] Buendia J A and Venkattraman A 2015 *Europhys. Lett.* **112** 55002
[18] Loveless A M and Garner A L 2017 *IEEE Trans. Plasma Sci.* **45** 574
[19] Loveless A M and Garner A L 2017 *Phys. Plasmas* **24** 113522
[20] Fu Y, Zhang P, Krek J and Verboncoeur J P 2019 *Appl. Phys. Lett.* **114** 014102
[21] Fu Y, Zhang P, Verboncoeur J P and Wang X 2020 *Plasma Res. Express* **2** 013001
[22] Garner A L, Meng G, Fu Y, Loveless A M, Brayfield R S and Darr A M 2020 *J. Appl. Phys.* **128** 210903
[23] Boyle W S and Kisliuk P 1955 *Phys. Rev.* **97** 255
[24] Forbes R G, Deane J H B, Hamid N and Sim H S 2004 *J. Vac. Sci. Technol.* B **22** 1222
[25] Khalifa M, Abdel-Salam M, Radwan R and Ali K 1977 *IEEE Trans. Power. Ap. Syst.* **96** 886
[26] Gossmann S *et al* 2018 *Proc. of the XXII Int. Conf. on Gas Discharges and Their Applications (Novi Sad, Serbia, 2–7 September 2018)* vol 1, ed Z Petrović (Serbian Academy of Sciences and Arts and Institute of Physics, University of Belgrade)
[27] Kaganovich I D, Demidov V I, Adams S F and Raitses Y 2009 *Plasma Phys. Control. Fusion* **51** 124003
[28] Tsendin L D 2010 *Phys. Usp.* **53** 133
[29] Xu L, Khrabrov A V, Kaganovich I D and Sommerer T J 2017 *Phys. Plasmas* **24** 093511
[30] Levko D, Arslanbekov R R and Kolobov V I 2019 *Phys. Plasmas* **26** 064502
[31] Robinson M 1969 *J. Appl. Phys.* **40** 5107
[32] Ferreira N G C, Almeida P G C, Benilov M S, Panarin V A, Skakun V S, Tarasenko V F and Naidis G V 2020 *IEEE Trans. Plasma Sci.* **48** 4080
[33] Bourdon A, Pasko V P, Liu N Y, Celestin S, Segur P and Marode E 2007 *Plasma Sources Sci. Technol.* **16** 656
[34] Popov N 2010 *Plasma Phys. Rep.* **36** 812
[35] Filippov A V, Derbenev I N, Dyatko N A, Kurkin S A, Lopantseva G B, Pal' A F and Starostin A N 2017 *J. Exp. Theor. Phys.* **125** 246–67
[36] Almeida P G C, Almeida R M S, Ferreira N G C, Naidis G V and Benilov M S 2020 *Plasma Sources Sci. Technol.* **29** 125005
[37] Kyritsakis A, Veske M, Eimre K, Zadin V and Djurabekova F 2018 *J. Phys. D: Appl. Phys.* **51** 225203
[38] Kaufmann H T C, Profatilova I, Popov I, Wuensch W and Benilov M S 2021 *9th Int. Workshop on Mechanisms of Vacuum Arcs (Online, 8–12 March 2021)*
[39] Lowke J J and D'Alessandro F 2003 *J. Phys. D: Appl. Phys.* **36** 2673
[40] Berger S 1976 *IEEE T. Power. Ap. Syst.* **95** 1073
[41] Feet O C, Seeger M, Over D, Niayesh K and Mauseth F 2020 *Energies* **13** 4449